Structural Feasibility Analysis of a Robotically Assembled Very Large Aperture Optical Space Telescope

W. Keats Wilkie, [*] R. Brett Williams,[†] Gregory. S. Agnes[‡], and Brian H. Wilcox[§]
Jet Propulsion Laboratory, California Institute of Technology, Pasadena, CA, 91109

This paper presents a feasibility study of robotically constructing a very large aperture optical space telescope on-orbit. Since the largest engineering challenges are likely to reside in the design and assembly of the 150-m diameter primary reflector, this preliminary study focuses on this component. The same technology developed for construction of the primary would then be readily used for the smaller optical structures (secondary, tertiary, etc.). A reasonable set of ground and on-orbit loading scenarios are compiled from the literature and used to define the structural performance requirements and size the primary reflector. A surface precision analysis shows that active adjustment of the primary structure is required in order to meet stringent optical surface requirements. Two potential actuation strategies are discussed along with potential actuation devices at the current state of the art. The finding of this research effort indicate that successful technology development combined with further analysis will likely enable such a telescope to be built in the future.

Nomenclature

α_T	=	Coefficient of thermal expansion, K^{-1}
C_{fl}	=	Reaction wheel dynamic imbalance constant, N/Hz^2
D	=	Diameter of primary reflector, m
δ_{dyn}	=	Surface deflection tolerance for dynamic disturbances, m
δ_{qs}	=	Surface deflection tolerance for static/quasistatic disturbances, m
Δl_{act}	=	Actuator stroke requirement, m
E	=	Young's modulus of truss structural elements, Pa
F	=	Focal length of primary mirror, m
f_c	=	Cutoff frequency of reaction wheel vibration isolation system, Hz
f_0	=	Fundamental natural frequency, Hz
$G_a(f)$	=	Disturbance acceleration power spectral density (PSD)
G_0	=	Disturbance acceleration PSD evaluated at f_0 , ($G_0 = G_a(f_0)$)
H	=	Depth of truss structure, m
η	=	Structural mass fraction of primary mirror, ($\eta = m_{truss}/(m_{truss} + m_{nonstuctural})$)
λ_{nom}	=	Nominal operational wavelength of telescope, m
$\lambda_{(s,n)}$	=	frequency parameter for (s,n) vibration mode of triangular mirror facet
M_{total}	=	Total telescope and spacecraft mass, kg
m_{truss}	=	Structural mass of truss (includes only longerons on the top and bottom of truss), kg
$m_{nonstructural}$	=	Nonstructural mass of primary mirror (includes mirror facets, and truss nonstructural mass), kg
N_{spc}	=	Number of struts per truss unit cell, -
ρ_{strut}	=	Density of truss strut material, kg/m^3
σ_e	=	Fabrication tolerance of structural elements, m/m RMS
T_U	=	Temperature of mirror facet for thermal analysis, K
T_L	=	Temperature of "moonshade" insulation for thermal analysis, K

[*] Senior Member, Technical Staff, Advanced Deployable Structures Group, MS 299-101, AIAA Member, william.k.wilkie@jpl.nasa.gov
[†] Member, Technical Staff, Advanced Deployable Structures Group, MS 299-101, AIAA Member.
[‡] Group Leader, Advanced Deployable Structures Group, MS 299-101, AIAA Associate Member.
[§] Project Principal Investigator, Autonomous Systems Architecture and Program Development Office, MS 303-310.

ΔT = Temperature differential of radiating surfaces enclosing truss, T_L - T_U, K
w_{RMS} = vertical displacement error of optical surface with respect to ideal surface, m RMS
ζ = Structural damping ratio, % critical

I. Introduction

There is interest in space-based telescopes with apertures that are far too large to use monolithic optical components. Therefore the use of segmented optics and deployable or on-orbit assembled structures has become commonplace in the realm of both Earth-observing and astronomical telescopes. This research effort focuses on a very large aperture optical space telescope that is assembled on-orbit by robots from structural cells that contain an optical reflector surface and components of the backing truss. This Earth-observing telescope will reside in a geostationary orbit and feature a 150-m diameter primary reflector along with the other optical surfaces shown in Figure 1.

While the sheer size of this primary mirror presents numerous engineering challenges in terms of the design, fabrication, testing, and on-orbit robotic assembly, the secondary and tertiary reflectors are large in their own right with diameters of 41.5-m and 63.5-m, respectively. Therefore, it is presumed that the technology development required to enable construction of the primary reflector will in turn be used for the smaller optical surfaces.

With the telescope system architecture specified in Figure 1, the feasibility of the primary mirror is now examined. First, the robotic assembly concept of the telescope is discussed, along with the facet cells that form the building blocks for the reflector. Then, surface precision requirements are used with appropriate ground and on-orbit loading scenarios identified in the literature to establish natural frequency requirements for both the individual optical facets as well as the primary mirror as a whole. These frequency requirements then determine the proper sizing of the optical facets and primary reflector. An estimate of the launch mass for the primary is made, including an investigation into the possibility of manufacturing facets with the desired areal density of 1-kg/m^2. The preceding analysis indicates that a passive truss support structure will not be able to meet the stringent optical surface finish requirements. Therefore, two options for actively control of the surface precision of the primary mirror are presented: direct control of the facet at its three corners and indirect control of the reflecting surface achieved by actively adjusting the length of the individual truss members. The performance of these two methods is compared along with a discussion of candidate actuator systems that are commercially available and have space-flight heritage. This effort concludes with an identification of the areas where further analysis and technology development are required in order to enable this type of large aperture optical telescope to be successfully designed and flown in space.

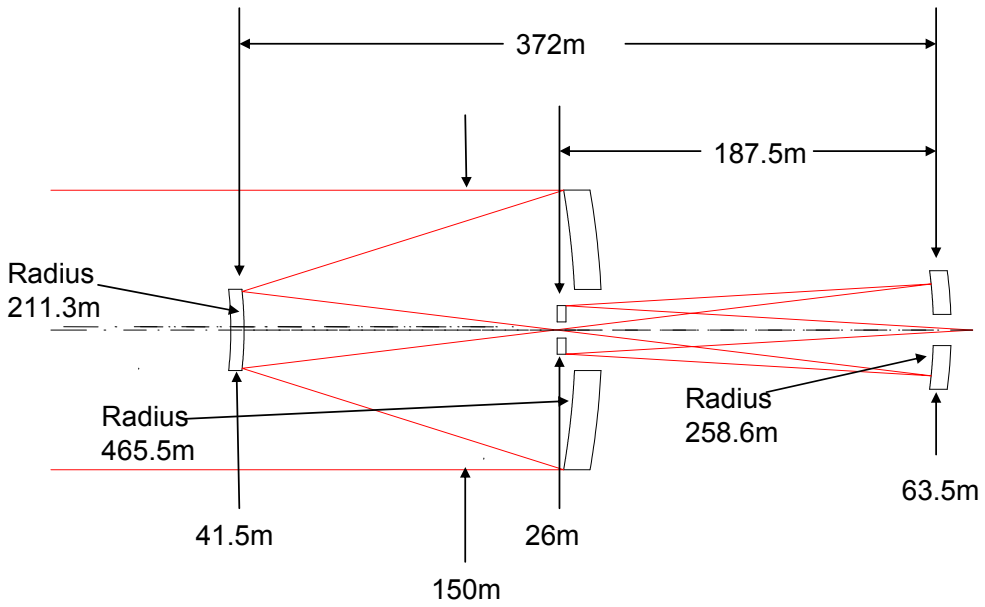

Figure 1: Configuration of Earth-Observing Optical Telescope with 150-m Primary Reflector.

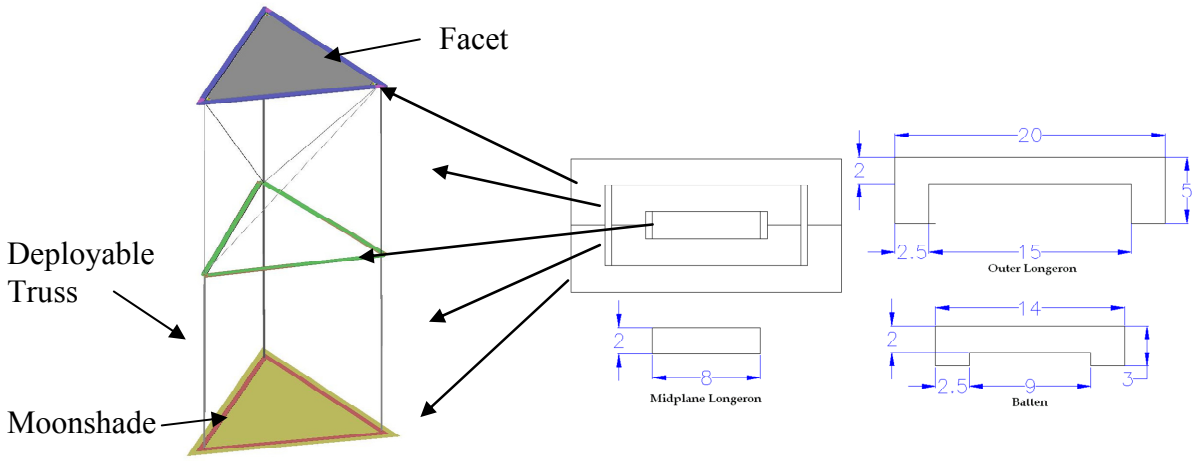

Figure 2: Deployed Facet with Supporting Truss and Proposed Nested Design for Supporting Truss.

II. Telescope Overview

A. Telescope Description

The general concept for this telescope involves mass producing a large number of identical, low-mass, low-cost optical facets with a deployable backing truss, seen in Figure 2, and launching them into orbit where they are assembled and adjusted by robots into large reflecting surfaces. The optical facets are triangular in shape, 2-m long on a side, and perimeter-supported by a triangular outer longeron frame. When stowed for launch, the supporting truss members nest into a 1-cm thick frame that surrounds the facet, as also depicted in Figure 2.

Figure 3 reveals some of the details of a facet cell. In addition to the nested truss members, the kinematic mounts for the facets, the piezoelectric strut length adjuster, and the indium-coated cup-and-cone connectors are depicted. The kinematic mounting system is designed to prevent transfer of structural loads into the facets. The piezoelectric strut adjustment system, which is discussed in more detail later, allows the robot to fine-tune the geometry of the structure in order to obtain the required RMS surface precision of the reflecting surfaces, which cannot be achieved passively due to limitations on the manufacturing and assembly of the truss components. The indium-coated cup-and-cone connectors are where one facet is joined to adjacent facets during the robotic assembly process. The connectors are magnetic, which applies enough force to cause the two indium-coasted surfaces to cold-weld together to form a permanent connection that does not exhibit microdynamic slippage during operation of the telescope. All of the non-electronic components of the telescope, including the mirror facets, their supporting truss elements, and the sunshield booms and membranes are sent into a low earth orbit (LEO) using one or two chemical rockets, where an electronic propulsion space tug will haul them into through the Van Allen radiation belts to a geostationary orbit (GEO). This two-part launch is energy efficient, and the longer period of time spent in the harsh radiation environment does not affect these passive structural components. At a later point in time, the active components, including the spacecraft bus, robots, focal planes, thrusters, and metrology components are launched separately on a chemical rocket directly into the desired GEO orbit. A geostationary orbit is chosen to capitalize on a more benign thermal environment and to eliminate slewing required to observe a specific point on the surface. This telescope in such an orbit provides 15-cm surface resolution with a stationary 500 km field of view and will require a large, lightweight, co-orbiting sunshield to shade the instrument. The robotic system then begins assembly of the telescope by first removing a facet cell from the stack of facet blanks and deploying its support structure, and then micromachining it in a metrology cell using an ion etching process to remove portions of a stress coating to give each panel its desired optical figure. Initial modeling suggests that only a small amount of etching over a few minutes is required to create the individual, custom aspherical surfaces from each facet. At this time, a robot adjusts the length of active truss members and/or the tip-tilt-piston of the facets to get the final primary surface within a range of real-time wavefront correction with hardware optically located between the tertiary reflector and the focal plane. Truss element lengths are adjusted using a "set and forget" microactuator system, which means a charge is applied to the actuator by the robot to change its length a certain amount, and after this charge is set, the robot can move onto its next task while the actuator retains is prescribed length. Because these actuators systems display some slow, time-dependent length changes, the robot is used to periodically adjust the truss by reenergizing the

actuators based on the results from a separate metrology system located at the focal point of the primary reflector. This metrology system is also used to perform real time control of the wavefront corrector facets discussed earlier. Potential actuator systems are discussed in more detail later. A robot then carries the facet cell as it crawls across the reflector surface, stepping in the "foot-holes" shown in Figure 3. Once at the correct location, the robot positions the facet cell and attaches it to the structure at the prescribed location, as shown in Figure 4.

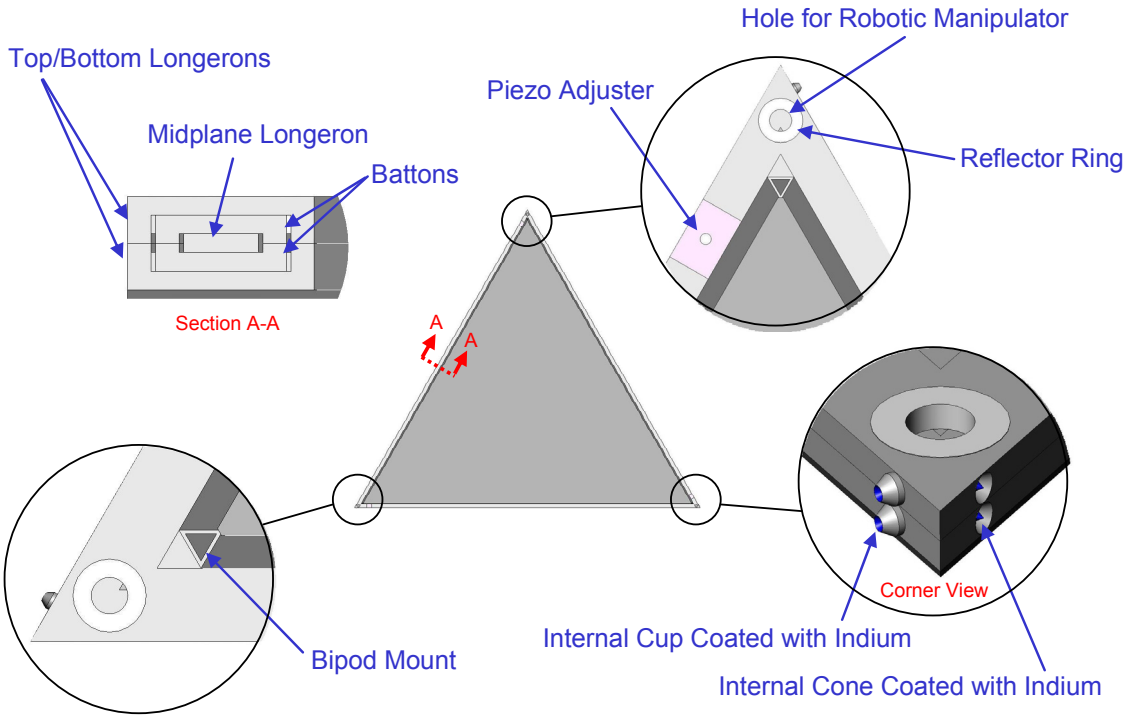

Figure 3: Optical Facet Assembly Details.

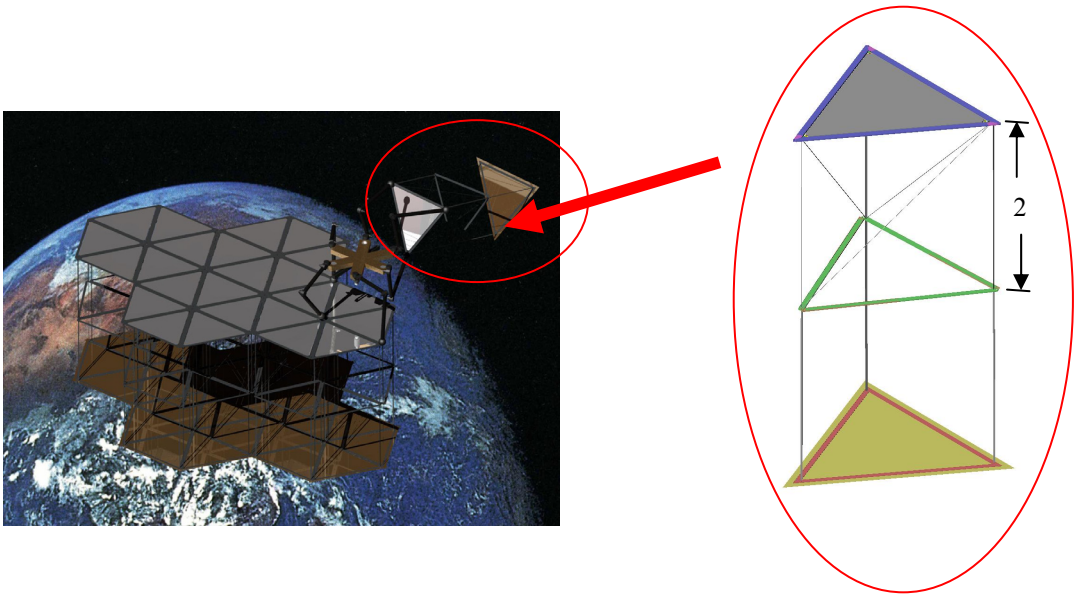

Figure 4: Deployed Facet Cell Being Assembled into the Reflector Structure.

In order to assemble the 150-m primary reflector in a reasonable amount of time, one facet cell must be adjusted and installed per hour. This timeframe is reasonable since etching of stress coating is predicted to take approximately 1 minute per spot to be etched. Also, one metrology/ion etching cell and set of robots may be used to build multiple telescopes over the span of several years to reduce overall mission costs.

B. Mass Considerations for Proposed Telescope

One of the most important considerations for space systems is the total system launch mass. The mass of this telescope system could be limited by launch vehicle capacity, or in the case of multiple launches, economic restrictions. For the telescope system under consideration, there are two main mass parameters of importance, which are addressed in the next two sections: the areal density of the optical facets and the overall mass of the primary reflector.

1. Mass Considerations for Optical Facets

In order to achieve this relatively low areal density, two types of optical facet materials are considered, both employing sandwich structure lightweight technology. The first sandwich structure is composed of silicon-carbide (SiC) face-sheets with a SiC foam core. The other has graphite-epoxy face-sheets with a graphite-epoxy honeycomb core. The current state of the art for foamed SiC facets is ~0.2-mm face sheets with 95% foam porosity. From Figure 5, it is clear that SiC foam technology will have to be improved in order to meet the desired 1-kg/m^2 facet areal density. For example, reducing the face-sheets to only 0.1-mm in thickness and increasing the porosity of the foam to 99% would result in the facet meeting the desired areal density. The graphite-epoxy facets have a lower coefficient of thermal expansion and are lighter than the SiC panels, and could therefore meet the desired areal density at a more reasonable porosity and face sheet thickness. However the facets made from graphite-epoxy have only half the stiffness of the SiC facets and are therefore unable to meet the facet frequency requirements for random vibrations discussed later.

2. Mass Considerations for the Telescope Primary Mirror

The 150-m diameter primary mirror is composed of some 9276 individual facets cells, each of which stows into a 1-cm thick package. For launch in a currently available launch vehicle, six of these stowed facets will be arranged in a hexagon pattern as shown in Figure 6.

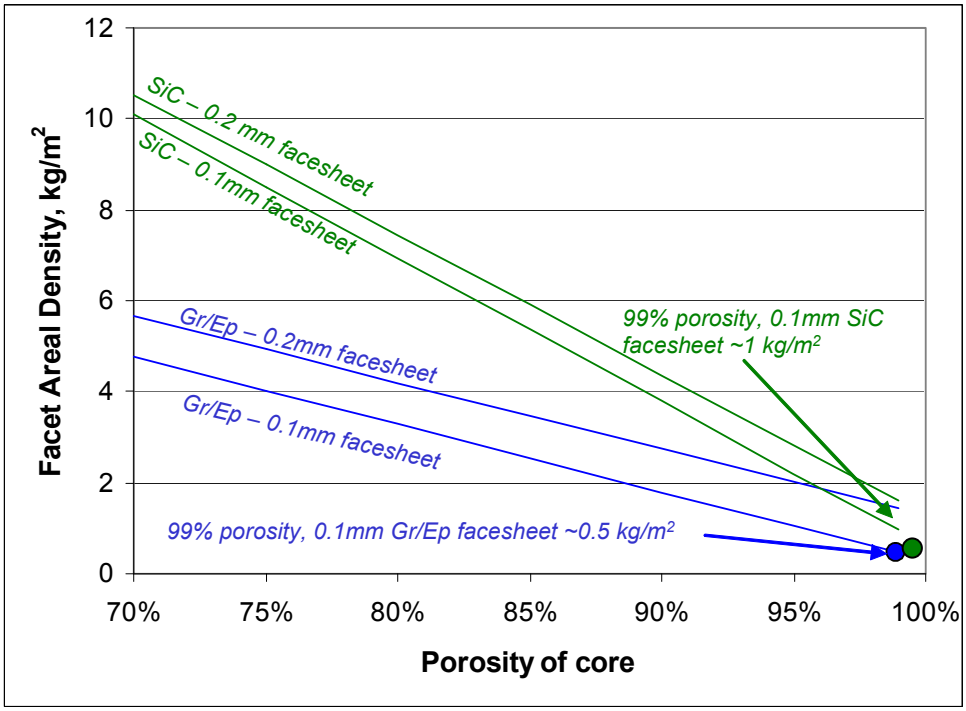

Figure 5: Achievable Areal Densities for Foamed SiC and Graphite-Epoxy Sandwich Optical Facets.

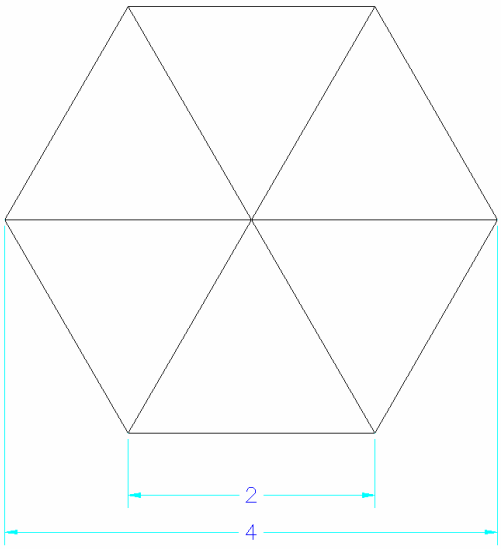

Figure 6: Launch Packaging of Primary Facets

This packing arrangement results in 1548 layers of stowed facet cells with a total stacked height of 15.5-m and a 161-m^3 stowed launch volume. This stack of facets will be preloaded in compression such that the launch loads are transmitted through the graphite-epoxy "frame" surrounding the optical facets, while the moonshields prevent the facets from making direct contact during launch. For the baseline 4-m deep truss, the launch mass of the primary mirror is estimated to be 32,971 kg. This mass gives an overall areal density of the primary mirror (total primary mass divided by total surface area) of 2.05 kg/m^2 for a nominal mass fraction η = 0.3 and a total stowed primary density of 205 kg/m^3.

One common launch vehicle for large payloads is the Delta IV, which has a fairing height of 12.2-m and a launch capability to low earth orbit (LEO) of 21,892 kg (or average payload density of 65 kg/m3). Based on these limitations, it is clear that multiple Delta IV launches and/or larger volume/lift capacity launch vehicles will be required in order to launch such a large primary mirror. Furthermore, more study is required to determine the launch requirements for the other components of the telescope system, such as facet cells required to assemble the subsequent reflecting surfaces, trusses to support the various mirror, and the telescope electronics and assembly robots.

III. Structural Requirements

In order to properly size and estimate the mass and structural performance of the telescope under consideration, it is first important to determine the RMS surface precision that must be maintained in order for the telescope to function properly. Then, the various types of loading scenarios that the system could be subjected to either on the ground or while on-orbit must be investigated. This section considers various potential disturbances that are common to space-based telescopes identified in the literature, and then uses the surface precision requirements to derive structural requirements on the fundamental frequency of both the optical facets as well as the complete primary mirror system.

A. Optical Facets

The primary mirror is composed of thousands of optical facets that must each individually meet certain structural requirements. This study considers two types of disturbances: static and dynamic. Self-loading due to gravity will be the only static disturbance discussed in this effort, while dynamic disturbances are due to random vibrations, telescope slewing, or onboard reaction wheels used for precision pointing control. For static loading the RMS surface accuracy requirement for visible light (λ_{nom}= 600 nm) is:

$$\delta_{g.t.} = 40\lambda_{nom} \Rightarrow 24\mu m$$

This requirement assumes that the fundamental mode dominates the response, resulting in sag that causes only a focus error that can be artificially corrected during testing. Thus, the RMS value is higher than is often associated with optical systems. The response of the structure to dynamic disturbances is often more complicated, so it is not possible to assume a first mode-dominated reaction. Therefore, a typical RMS surface accuracy requirement for an optical telescope mirror surface is:

$$\boxed{\delta_{dyn} = \lambda_{nom}/15 \Rightarrow 40nm}$$

It is also assumed that the optical facets will have 0.5% structural damping for this initial study.

There are two main scenarios where the facets will encounter these various disturbances, on the ground prior to launch and on-orbit after assembly. These two loading scenarios are discussed in the two subsequent sections.

1. Requirements based upon Ground Testing Constraints

In order for a structure subjected to a uniform 1-g acceleration to meet or exceed its static RMS surface accuracy requirement, it must have a fundamental frequency given by (Peterson and Hinkle 2005)

$$f_0 > \sqrt{\frac{g}{4\pi^2 \delta_{g.t.}}} \tag{1}$$

For this set of requirements, the minimum fundamental frequency requirement of an individual optical facet for ground testability is found to be 102 Hz. It should be noted that this equation is independent of any geometric or material properties of the structure. It simply states that whatever structure is being considered, it must be designed to have such a fundamental frequency in order to meet the static RMS requirement.

During ground testing of a structure, the dominant dynamic disturbance will be vibrations introduced by the test environment. Assuming a random disturbance spectrum with a 10 μg rms amplitude and 0-100 Hz bandwidth, and a conservatively low structural damping of 0.5%, the structure will require a minimum fundamental frequency of (Peterson and Hinkle 2005)

$$f_0 > \frac{1}{2\pi}\sqrt[3]{\frac{G_{0_{ground}}}{8\zeta\delta_{dyn}^2}} = 18.2Hz \tag{2}$$

where G_0 is the magnitude of the disturbance PSD evaluated at f_0, i.e.

$$G_{0_{ground}} = G_{a_{ground}}(f_0) = (9.81\times10^{-5})^2 \frac{1}{100} \quad \frac{g^2}{Hz} \tag{3}$$

2. Requirements Based on On-Orbit Dynamics

While on orbit, pointing requirements could subject the individual optical facets to quasi-static slewing accelerations. For a very slow, but reasonable, slew acceleration of 10^{-8} m/s^2, the facets must have a fundamental frequency of

$$f_0 > \sqrt{\frac{10^{-8}}{4\pi^2 \delta_{dyn}}} = 0.25Hz \tag{4}$$

in order to meet its dynamic RMS surface accuracy requirement.

Also while on-orbit, the facets could experience random vibration disturbances similar to those encountered during ground testing. However, anticipated accelerations in space are lower, perhaps around 1 μg over the same 0-100 Hz bandwidth. Therefore, on-orbit

$$G_{0_{orbit}} = (9.81\times10^{-6})^2 \frac{1}{100} \quad \frac{g^2}{Hz} \tag{5}$$

and the fundamental frequency requirement is

$$f_0 > \frac{1}{2\pi}\sqrt[3]{\frac{G_{0_{orbit}}}{8\zeta\delta_{dyn}^2}} = 3.9Hz \tag{6}$$

3. *Analysis of Facet Structural Dynamics*

Vibration of triangular facets. As ground testing was not a requirement, on-orbit disturbances became the primary structural stiffness design driver for the mirror facets. The on-orbit dynamics environment analysis determined a minimum vibration frequency requirement for each of the triangular mirror facets assuming vibrational disturbances originating from quasi-static slewing accelerations and random sources. Disturbances from random on-orbit vibrations resulted in the higher minimum frequency (3.9 Hz). To keep resulting dynamic deflections within optical performance limits, the mirror facet must be designed such that its minimum fundamental vibration frequency is greater than or equal to 3.9 Hz (from Eqn.6).

Given the geometric constraints on the mirror facets (2m equilateral triangles with a maximum thickness of 0.01m), a parametric study was performed where the fundamental vibrational mode of the triangular facet panels was calculated as a function of silicon carbide face sheet thickness and foamed silicon carbide foam core density. Trends for pinned vertices, free edges, simply-supported and clamped boundary conditions were evaluated using finite element analysis. Results for the limiting case of a zero-density core material are shown in Figure 7. The shaded region indicates the space where both facet minimum stiffness and areal mass density constraints are satisfied. The analysis shows that, if facet mass is constrained to be less than or equal to 1kg/m^2, pinned vertex mounting, or mounting approximating free edge boundary conditions, will not meet the minimum frequency requirement. A facet simply supported on all edges appears minimally capable of meeting the 3.9 Hz requirement. Clamped boundaries exceed the minimum requirement.

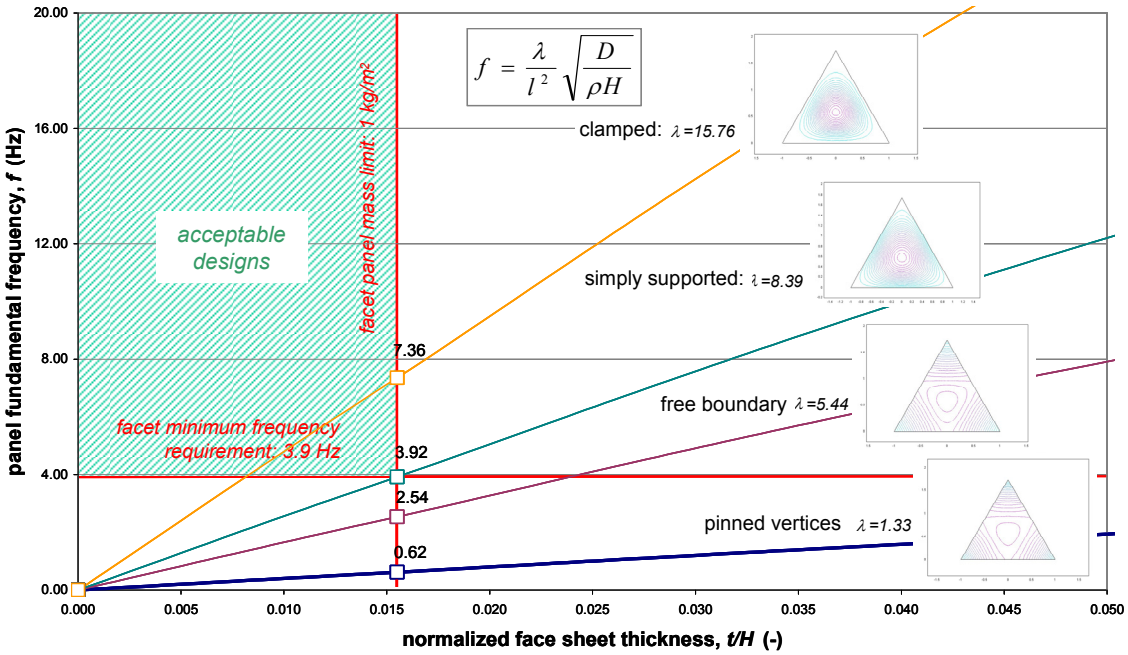

Figure 7. Fundamental vibration characteristics of mirror facets as a function of face-sheet thickness and boundary conditions.

Given that the addition of a non-zero mass facet core will reduce the acceptable design space further by decreasing the maximum allowable face sheet thickness, mirror facets will need boundary conditions approaching the clamped case. This could be accomplished by a continuous or piecewise bonding of the facet edges to the outside supporting frame. Alternatively, the facet panel structure could be constructed with a stiffened edge and thinned interior. Both scenarios, which could be studied as part of a detailed design study, appear to offer plausible, realizable solutions capable of meeting the on-orbit dynamics requirements for the facet structural design.

B. Primary Mirror

Above the requirements for the individual optical facets were determined. In this section, the entire primary mirror is considered as its own structure in order to determine its fundamental frequency requirements and thus estimate its depth and mass. As was the case with the individual facets considered, the primary could be subjected to uniform gravity loads (static) or dynamic disturbances either on the ground or on-orbit. This section considers these various loading scenarios and determines the appropriate frequency requirements for the primary reflector.

1. Requirements Based upon Ground Testing Constraints

Figure 8 shows a schematic of the primary mirror in a 1-g ground testing environment and the resulting gravity sag. In order to meet the ground testing requirements specified above, the fundamental frequency of the primary mirror is subject to the constraint

$$f_0 > \sqrt{\frac{g}{4\pi^2 \delta_{g.t.}}} = 102 Hz \tag{7}$$

If the primary reflector was constructed and tested on the ground, it would again be subjected to random vibrations from the surrounding test environment. From above, for a disturbance level of 10 μg over the frequency range 0-100 Hz,

$$G_0 = (9.81 \times 10^{-5})^2 \frac{1}{100} \tag{8}$$

and assuming 0.5% structural damping, the required frequency of the primary reflector is

$$f_0 > \frac{1}{2\pi} \sqrt[3]{\frac{G_{0_{ground}}}{8\zeta \delta_{dyn}^2}} = 13.9 Hz \tag{9}$$

Because these required fundamental frequencies are so large, it is clearly not reasonable to ground-test a 150-m diameter primary mirror. To do so would require a significantly deeper support truss with a much higher mass and more complex deployment/assembly methodology.

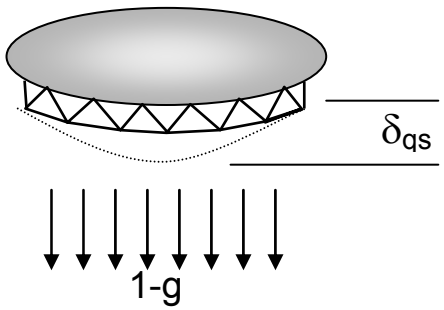

Figure 8: Primary Mirror under 1-g Loading During Ground Testing

2. Requirements Based on On-Orbit Dynamics

Spacecraft vibration sources and random disturbances. The telescope structure, and in particular, the primary mirror backing structure, will be subject to various vibrational disturbances on orbit. These disturbances can cause unacceptably large deflections in the telescope mirror surface if the supporting structure is insufficiently stiff. It is convenient to characterize the structural stiffness of the mirror structure by its fundamental frequency of vibration. For conceptual design studies, the mirror structure may be idealized as a thin circular plate with free edges. Its resulting natural frequencies may then be directly calculated from straightforward analytical solutions. For a circular, relatively flat, tetrahedral truss structure supported freely at the edges, the vibrational frequencies are given by

$$f_{(s,n)} = \lambda_{(s,n)}^2 \left(\frac{3}{\sqrt{2}} \right) \left(\frac{H}{D^2} \right) \sqrt{\frac{E\eta}{\rho_{strut} N_{spc}}} \tag{10}$$

Here, H is the truss depth, D the overall diameter of the structure, E and ρ_{strut} are the Young's modulus and density of the truss structural elements, and η is the structural mass fraction of the entire mirror structure, defined by

$$\eta \equiv \frac{m_{truss}}{m_{truss} + m_{nonstructural}} \tag{11}$$

where m_{truss} is the structural mass of the truss, i.e., the mass of all components providing stiffness, and $m_{nonstructural}$ is the mass of all other components, including truss joints and the mass of the mirror facets themselves. N_{spc} is the number of assumed structural elements per truss unit cell. For the truss cell configurations examined in this study, a value of $N_{spc} = 6$ was selected. The frequency parameters, $\lambda_{(s,n)}$ for the free circular plate may be obtained from tabulated sources, e.g., Leissa.

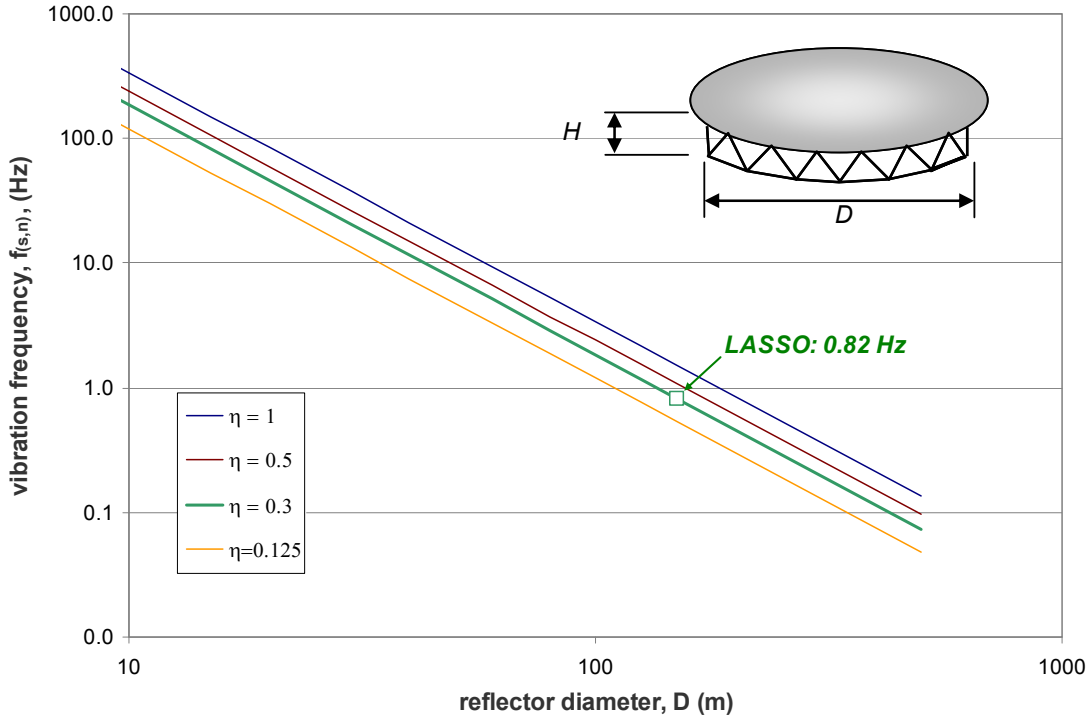

Figure 9: Fundamental vibration frequency of telescope primary mirror as a function of aperture diameter and structural mass fraction. H = 4m assumed.

As the lowest vibrational mode is typically the most significant, it is evaluated here in detail. Trends for the fundamental mode frequency as a function of the primary reflector diameter, D, and structural mass fraction, η, are shown in Fig. 9. Truss depth, H, was held constant at the nominal configuration truss depth of 4m. The nominal frequency of the 150m diameter primary reflector for its estimated structural mass fraction of 0.3 is approximately 0.82 Hz.

One typical source of spacecraft vibrations are attitude control reaction wheels. Minor imbalances in the reaction wheels result in oscillatory loads at the reaction wheel rotational frequency. Proper dynamic isolation of the reaction wheels can limit, although not necessarily eliminate, propagation of this vibrational energy into the telescope instrument. The dynamic response of the telescope mirror structure may be estimated as a function of the expected reaction wheel imbalance load, the dynamic characteristics of the isolation system, and the overall inherent structural damping of the mirror structure. Given the maximum tolerable deflection amplitude for the mirror surface, typically expressed as a multiple of the nominal telescope operating wavelength, a stiffness requirement for the backing structure may be derived in terms of its fundamental vibrational frequency. If the fundamental vibrational frequency of the mirror is above a certain threshold, then the resulting disturbance amplitude should be within tolerable limits. Peterson and Hinkle give the relationship for the minimum structural frequency, f_0, as

$$f_0 > f_c \sqrt{\frac{C_{f1}}{M_{total}} \frac{4\sqrt{2}}{4\pi^2 \delta_{dyn}} \frac{1}{2\zeta} - 1} \tag{12}$$

where f_c is the cut-off frequency of the reaction wheel dynamic isolation system, C_{f1} is the reaction wheel imbalance load, M_{total} is the total mass of the telescope and spacecraft, ζ is the structural damping of the mirror structure, and δ_{dyn} is the maximum permissible dynamic response amplitude of the mirror surface. Nominal reaction wheel parameters used in this study are given in Table 1. The resulting minimum frequency required for the primary structure is 0.23 Hz. This is well below the nominal primary frequency of 0.82 Hz, therefore reaction wheel imbalance vibrations are not expected to be a major concern.

Vibrational disturbances from unspecified, generally random, sources are also an operational concern. As with reaction wheel vibrations, a minimum acceptable mirror vibrational frequency can be determined given the anticipated random disturbance spectrum. The minimum structural frequency for random vibration disturbance rejection is given by

$$f_0 > \frac{1}{2\pi} \sqrt[3]{\frac{G_0}{8\zeta \delta_{dyn}^2}} \tag{13}$$

where G_0 is the random disturbance power-spectral density RMS amplitude (assumed constant over the bandwidth of interest) evaluated at f_0, ζ is the inherent structural damping of the structure, and δ_{dyn}, again, is the maximum tolerable dynamic response amplitude of the mirror surface.

The resulting minimum frequency requirement of the primary mirror is shown as a function of random disturbance amplitude and structural damping in Fig. 10. A 0-100 Hz disturbance bandwidth was assumed. For a conservative structural damping of 0.5%, the nominal 150m telescope configuration, which has a fundamental mode frequency of 0.82Hz, should be able to tolerate random disturbances on the order of 0.1 micro-g RMS. This is a very low level of vibration, but given the anticipated small disturbance GEO environment, perhaps reasonably achievable.

Table 1. Reaction wheel vibration parameters

parameter	value
Dynamic isolation cut-off frequency, f_0	0.1 Hz
Reaction wheel imbalance	0.4 gm-cm
Reaction wheel imbalance load, C_{f1}	1.6×10^{-4} N/Hz^2
Total system mass (spacecraft + primary), M_{total}	34000 kg
Mirror surface dynamic amplitude tolerance, δ_{dyn}	$\lambda_{nom}/15 = 40$ nm
Inherent structural damping of truss, ζ	0.5% critical
Total number of reaction wheels	4

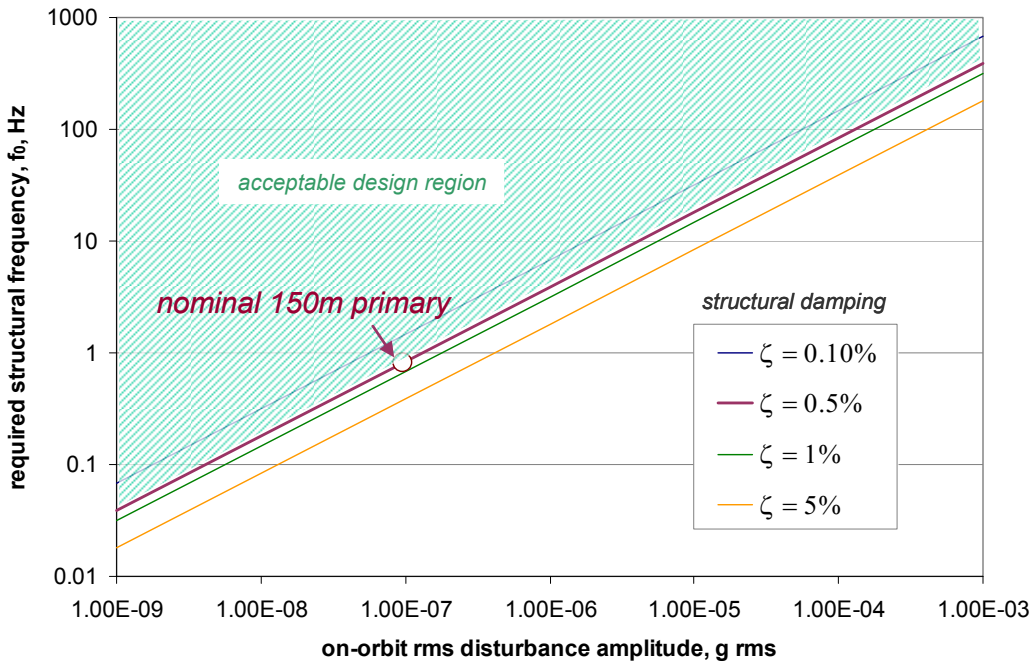

Figure 10. Primary mirror frequency required for random on-orbit vibration disturbance rejection.

3. Requirements Based on Thermal Distortion of the Primary Mirror

Curvature distortion due to thermal gradients. Although the 150m telescope will be operating behind a co-orbiting sunshade at all times, small variations in incident heating, e.g., due to Earth albedo, or relative position of the sunshade with respect to the telescope, can be expected to produce minor thermal gradients within the backing structure of the primary mirror. These thermal gradients can cause a resultant distortion of the mirror curvature, which may or may not be easily correctable. From Hedgepeth, the following expression for the expected root-mean-squared variation of a mirror surface due to thermal gradients across the faces of a backing truss structure may be developed:

$$w_{rms} = \frac{\alpha_T (T_L - T_U)}{H} \frac{1}{\sqrt{48}} \left(\frac{D}{2}\right)^2 \tag{14}$$

α_T is the coefficient of thermal expansion of the truss structural elements and $T_L - T_U$ is the temperature difference between the lower truss face elements and the upper face elements located nearest the mirror panels. The backing truss structure here is assumed to be located between two radiating surface, i.e., the mirror surface and a lower layer of insulation or "moon shade" material, as shown in Figure 11.

This analysis assumes that temperature variations from the overall equilibrium temperature of the structure are comparatively small, that all surfaces have an emissivity of 1, and that there is no thermal conduction within the structure. $T_L - T_U$ further may be derived in terms of the temperature difference of the enclosing radiating surfaces, ΔT, as

$$T_L - T_U = \frac{\frac{1}{2} - f_1\left(\frac{H}{F}\right) + k\frac{2\sqrt{3}d}{l}}{1 + k\frac{2\sqrt{3}d}{l}} \Delta T \tag{15}$$

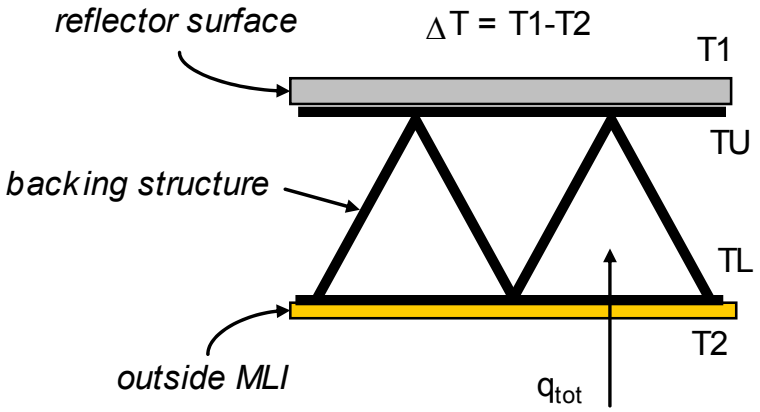

Figure 11: Thermal arrangement of primary mirror backing truss.

where f_1 accounts for the varying view factor of truss elements to the curved radiating surfaces, and is given by

$$f_1\left(\tfrac{H}{F}\right) = \frac{1}{2}\left[1 - \frac{\sqrt{\left(\tfrac{H}{F}\right) + \left(\tfrac{H}{F}\right)^2 / 4}}{1 + \left(\tfrac{H}{F}\right)/2}\right] \tag{16}$$

H/F is the ratio of truss depth, H, to primary mirror focal length, F. The mirror surface is assumed to have spherical curvature with F equal to ½ the radius of curvature. The *k*-term in Eqn. 15 accounts for the view blockage due to intervening truss elements. Note that for a flat truss (zero curvature) without inter-truss blockage ($k = 0$), the upper and lower truss faces will be at the same temperature and no net curvature distortion occurs.

Substituting Eqns. 15-16 into Eqn. 14, and expressing the surface rms distortion in terms of the allowable wavefront error of the mirror, yields the following expression for the maximum thermal-distortion-limited primary mirror diameter:

$$\frac{D}{\lambda_{nom}} = \frac{4\sqrt{48}}{\alpha_T \Delta T} n_{tol} \frac{H}{D}\left[\frac{1 + k\frac{2\sqrt{3}d}{l}}{\frac{1}{2} - f_1\left(\tfrac{H}{F}\right) + k\frac{2\sqrt{3}d}{l}}\right] \tag{17}$$

This is plotted as a function of $\alpha_T \Delta T$ for a number of truss depth ratios (H/D) in Figure 12 for a wavefront error tolerance of $2\lambda_{nom}$ ($n_{tol} = 2$). For the 150m telescope concept with focal length F = 233 m, nominal strut diameter d = 0.01m, face strut length l = 2m, and a blockage correction factor k = 2, D/λ is 6.0×10^{-8}, which results in a maximum tolerable $\alpha_T \Delta T$ of 0.6×10^{-7}.

Given a reasonably achievable α_T of 0.5×10^{-6} for all strut elements, the overall temperature gradients on the mirror structure will need to be kept below 0.1K to keep curvature distortion of the primary mirror to within acceptable limits. This will be an engineering challenge. A more detailed thermal analysis, including orbital heating and sunshade effects, will be required to determine the exact thermal environment and resulting thermal distortions are manageable.

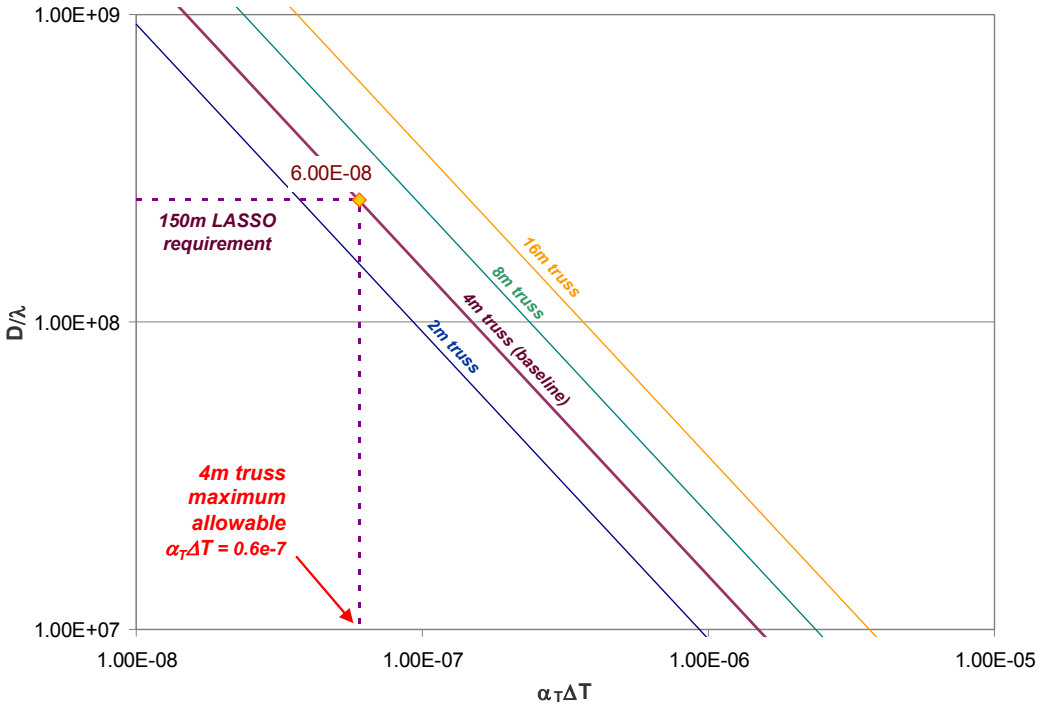

Figure 12: Maximum curvature-distortion-limited mirror aperture as a function of $\alpha\Delta T$ across mirror backing truss structure. $2\lambda_{nom}$ wavefront error tolerance assumed.

4. Requirements Based on Manufacturing and Assembly Precision

Surface distortions due to fabrication tolerances. The backing structure of the primary mirror must not only provide stability against dynamic disturbances, but must also establish and maintain the general arrangement of the mirror facets to within some optically defined tolerance. A perfectly manufactured and precisely assembled structure will accomplish this implicitly. However, structural perfection is not achievable in practice, and small manufacturing errors in the dimensions of the truss structural components will lead to a variation in the desired surface geometry.

An estimation of the expected root-mean-squared vertical deviation of the surface of a truss structure from its ideal shape can be found as a function of manufacturing tolerances using Hedgepeth's approach. For relatively flat, tetrahedral trusses of circular planform with free edge conditions, the expected out-of-plane RMS distortion of the truss face surface, normalized by the overall diameter, is given by

$$\frac{w_{rms}}{D} = \sqrt{\left[0.119\frac{l}{H}\right]^2 + \left[G_1\left(\tfrac{l}{H}\right)G_2\left(\tfrac{l}{D}\right)\frac{l}{H}\right]^2}\,\sigma_\varepsilon \tag{18}$$

where D is the mirror diameter, l/H is the ratio of truss face element length to truss depth, and σ_ε is the manufacturing tolerance of the truss structural elements. G_1 and G_2 are transverse shear terms applicable to very deep trusses. For the present study, these terms are small and may be neglected, in which case Eq. 18 reduces to

$$\frac{w_{rms}}{D} \approx 0.119\frac{l}{H}\sigma_\varepsilon \tag{19}$$

The maximum allowable displacement error in the mirror surface, as before, will be specified by telescope optical performance requirements and may be characterized as some multiple or fraction of the telescope nominal wavelength, or

$$w_{rms} = n_{tol}\lambda_{nom} \tag{20}$$

For purely passive optical systems, n_{tol} would typically be on the order of 1/50 or less of a wavelength. The current 150m concept is assumed to use an advanced active wavefront correction system, which considerably relaxes this constraint, and the maximum permissible distortion of the primary mirror surface is permitted to be two wavelengths (n_{tol} = 2). Substituting Eqn. 20 into Eqn. 19 provides us with the following useful relationship:

$$\frac{D}{\lambda_{nom}} = 8.4\frac{n_{tol}}{\sigma_\varepsilon}\left(\frac{H}{l}\right) \tag{21}$$

Equation 21 describes the upper limit on telescope aperture size, D, as a function of wavefront error tolerance, n_{tol}, truss structural depth, H, truss face element length, l, and manufacturing tolerance σ_ε, for any nominal optical wavelength, λ_{nom}. This telescope performance limit is plotted as a function of manufacturing tolerance for a variety of truss depth ratios in Figure 13. A wavefront error tolerance of n_{tol} = 2, consistent with the 150m telescope case under study, was assumed. A horizontal line indicating the D/λ performance requirement for the 150m concept is also indicated.

Manufacturing tolerances of 10e-4 are representative of precision routinely achievable in high quality machine shops. 10e-5 is consistent with more expensive manufacturing techniques utilizing hard tooling. 10e-6 tolerances are possible through extraordinary efforts, although at extremely high cost. From examination of Fig. 13 it is evident that no combination of reasonable truss depth or precision manufacturing will be capable of achieving the 150m telescope performance requirement with a purely passive structure. Alternatives employing various distributed actuation systems to overcome this limitation are discussed in the following section.

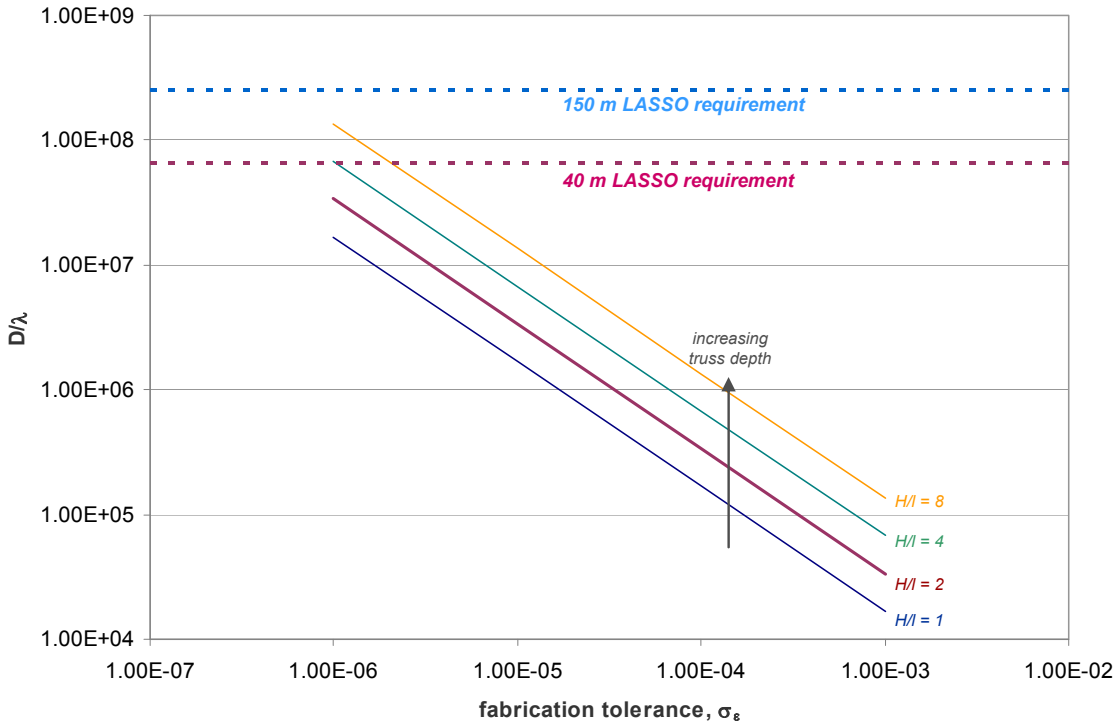

Figure 13: Surface error limited telescope size as a function of manufacturing tolerances and truss depth. Wavefront error n_{tol} = 2 assumed. (λ_{nom} = 600 nm for the 150m concept.)

IV. Quasistatic Active Control Strategies

Given the strong influence of manufacturing tolerance errors over achievable mirror diameter, some means of correcting the resulting surface distortions of the mirror will be required. Piezoelectric actuators have been successfully used for controlling vibrations and dynamics on various structures, including some space structures. For the present application, strategically distributed piezoelectric stack actuators could potentially be used to correct the surface distortion of the primary mirror surface. Piezoelectric stack actuators are also commercially available from a number of vendors and in a variety of material compositions, are easily customized to particular application specific geometries, and many examples have flown in space. Two conceptual possibilities utilizing piezoelectric or electrostrictive stack actuators for static deflection control are discussed here. For mechanical and analytical simplicity, only direct strain actuation approaches are considered.

A. Direct Displacement Control of Mirror Facets

The most obvious direct strain actuation approach to correct out-of-plane surface errors is to place piezoelectric stack actuators at the vertices of each mirror facet (Figure 14). The vertex vertical displacements of each facet may then be adjusted to within some tolerance of the optimal primary mirror surface. This approach is analogous to a "tip-tilt-piston" correction system on some active mirror systems.

The required stroke for each actuator will be of the same order as the rms surface displacement error given in Eqn. 19, i.e.

$$\Delta l_{act} \propto w_{rms} = 0.119 \frac{l}{H} \sigma_{\varepsilon} D \tag{22}$$

A plot of the surface rms error, which must be corrected by the actuators, is given in Figure 15 for several truss depth ratios. For a reasonable fabrication tolerance of σ_ε = 10e-5, and the nominal truss depth of 4m, the 150m telescope would require vertex actuators with stroke capability on the order of ±89μm to reduce the rms surface errors to within the telescope performance limit of 1.2 μm.

Assuming mirror facet packaging constraints limit the amount of vertical space available for each actuator to 1cm, piezoelectric materials capable of producing order of 1% strains would be required, which is well beyond the current state of the art for engineering piezoceramics (order of 0.1%). Actuators employing displacement amplification mechanisms may be designed to overcome this limitation, although at the cost of greater complexity and perhaps mass.

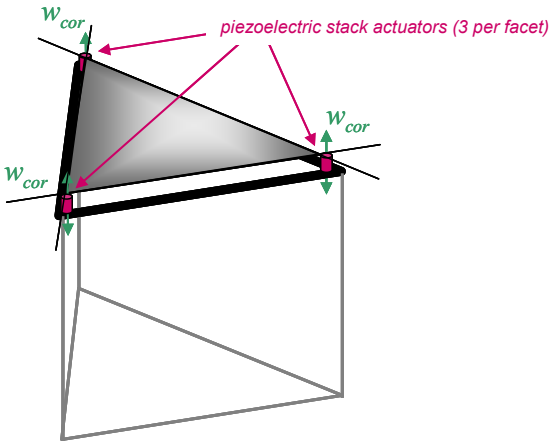

Figure 14: Compensation of surface distortion via direct adjustment of mirror facet vertex height.

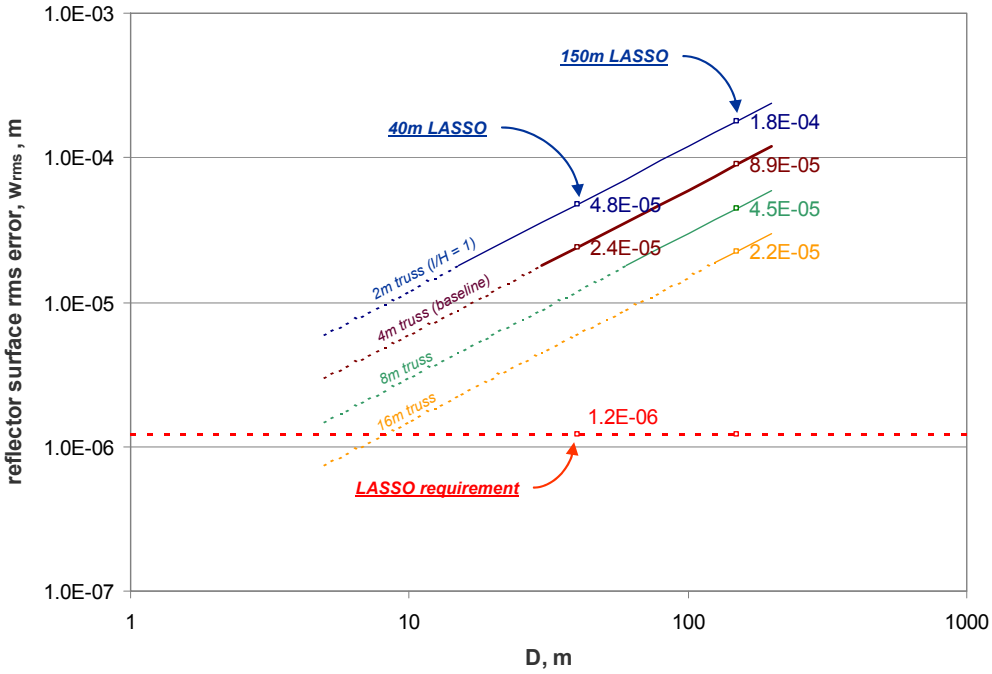

Figure 15: Mirror truss rms surface error versus mirror diameter. σ_ε = 10e-5 assumed.

B. Active Strut-Length Error Correction

As an alternative to correcting displacement errors of the mirror facet vertices directly, it may be possible to correct the length errors in individual truss elements, thereby eliminating unwanted rms surface distortions at the source. This would be accomplished by building piezoelectric stack actuators into each strut. Once deployed the lengths of each strut may be electronically adjusted to reduce or eliminate random length variations. This approach is illustrated conceptually in Figure 16.

Required stroke capability for the embedded strut actuators will be proportional to the strut manufacturing tolerance, σ_ε, and the overall strut length, l, i.e.,

$$\Delta l_{act} \propto l\sigma_\varepsilon \tag{23}$$

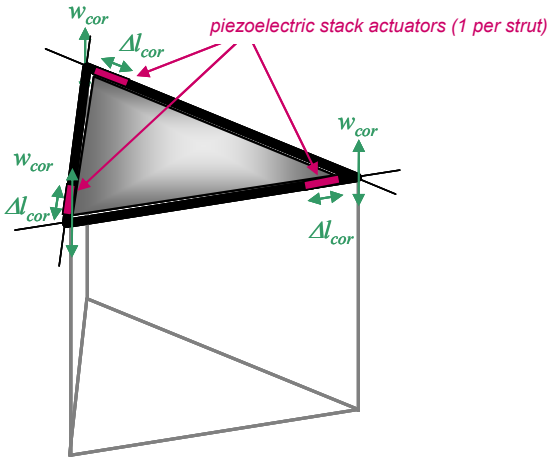

Figure 16. Correction of surface distortion via strut length adjustment.

In the case of the 150m telescope, with 2m struts on the truss faces and a σ_ε = 10e-5, this results in an actuator stroke requirement on the order of ±20 μm. This is achievable with present day piezoelectric ceramics using stacks of only one to two centimeters in length. It is also interesting and important to note that, in contrast to the vertex displacement correction approach, this actuator stroke requirement is independent of mirror diameter. As aperture size increases, however, the accuracy to which the actuators must be set will increase. Strut length error correction may be incorporated into Eqn. W-12 to give us an equation for maximum achievable telescope diameter using an active truss structure as follows:

$$\frac{D}{\lambda_{nom}} = 8.4 \frac{n_{tol}}{\sigma_\varepsilon \cdot \sigma_{act}} \left(\frac{H}{l} \right) \tag{24}$$

where σ_{act} is defined as the actuator setting accuracy divided by overall actuator stroke. Trends in surface error limited telescope mirror size versus fabrication tolerance for an active truss structure are shown in Figure 17. Curves for the passive structure alone, as well as curves assuming various degrees of actuator setting accuracy are indicated. These results indicate that with a reasonable fabrication precision of 10e-5, a 0.01 actuator setting accuracy would be capable of correcting a 4m truss structure to within the 150m performance requirement. With the appropriate metrology system in place, this level of precision should be achievable with current piezoelectric or electrostrictive materials.

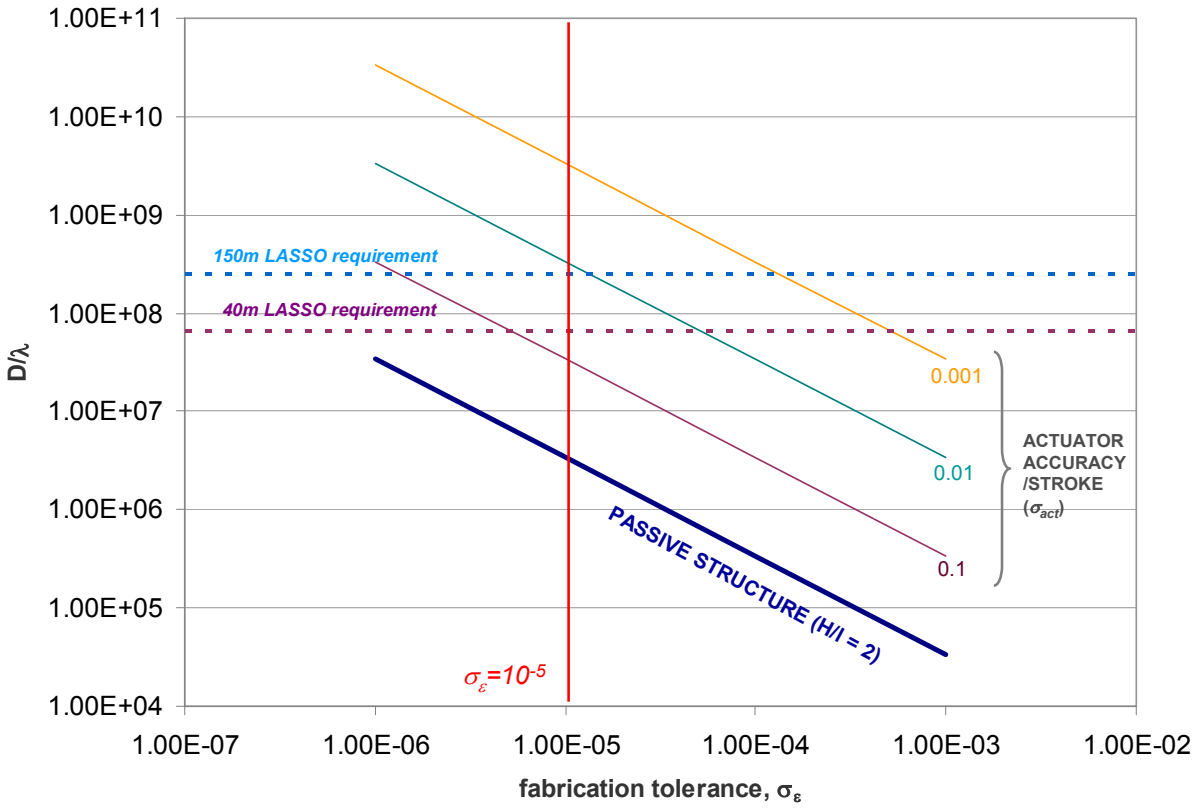

Figure 17: Surface-error-limited primary mirror diameter for backing truss with active strut-length error correction. 2λ wavelength error assumed.

C. Operational considerations for distributed actuation control

Although, in principle, an active strut length error correction approach appears capable of satisfying the 150m telescope mirror surface precision requirements, many practical challenges remain to effectively incorporate such a system on a very large spacecraft structure. Perhaps most immediately, the problem of providing power to every actuator must be addressed. For the 150m telescope primary, wiring harnesses would be cumbersome and heavy, as well as complicate the robotic deployment and assembly sequence.

Since active vibration control is not necessary for this particular application, a simpler approach would be to take advantage of the capacitive nature and low leakage properties of the piezoelectric actuators and locally set each device to the proper length during initial on-orbit assembly. Piezoelectric materials are capable of setting and holding a static position given a stored electric charge. Creep is dependant on material composition and temperature, as well as charge leakage, but occurs on generally logarithmic time scales, and a maintenance robot, as envisioned for this telescope concept, could periodically refresh the charge on individual actuators about the truss structure to maintain the required surface precision.

An alternative "power-off" set-and-hold strategy would be to reset the initial polarization strain of individual piezoelectric stacks to an intermediate position corresponding to the desired length. The electric field cycling process required to perform this is illustrated qualitatively in Figure 18 for a PLZT piezoelectric material composition. Creep behavior in the set polarization strain also exhibits a log-time behavior, but over sufficiently long time scales to be useful in static positioning application.

Creep phenomenon, polarization characteristics and stability of piezoelectric and electrostrictive materials are, to a large extent, research areas. Piezoelectric properties in particular are strongly dependent on temperature. For example, piezoelectric strain coefficients, and hence stroke capability, typically decrease with temperature. Polarization stability, hysteresis, and creep characteristics tend to improve however. As the nominal operating temperatures for the 150m telescope is expected to be in the vicinity of 150K, accurate prediction of piezoelectric behavior at these conditions will be necessary at a minimum to properly sizing of the actuator stacks. Both set-and-hold methods could benefit from an experimental study to more completely characterize long-term creep behavior of piezoelectric stacks at representative thermal conditions.

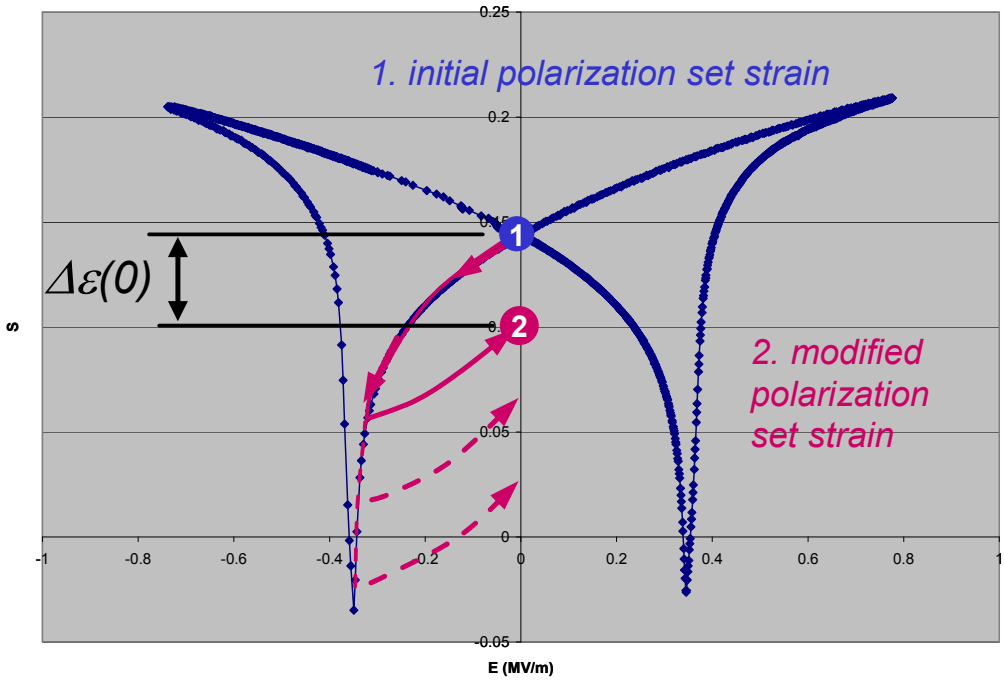

Figure 18: Polarization strain resetting for static position control using a PLZT composition.

Conclusions

This study identified a 150-m diameter primary mirror optical telescope architecture was identified and preliminary sizing was performed using rational design rules. Several key technologies and system design drivers were identified. 1 kg/m^2 silicon carbide mirror segments, quasistatic solid-state structural adjustment, indium cold-weld magnetic latches and facet cell deployment. Also more detailed study of the thermal environment and telescope systems engineering is required. Successful technology development and further study should enable large geosynchronous earth-observing telescopes.

Acknowledgments

The research described in this paper was carried out at the Jet Propulsion Laboratory, California Institute of Technology, under a contract with the National Aeronautics and Space Administration, and with funding from Defense Advanced Research Projects Agency.

References

[1]Peng, C-Y, Levine, M., Shido, L., Jacoby, M., and Goodman, W., "Measurement of Vibrational Damping at Cryogenic Temperatures for Silicon Carbide Foam and Silicon Foam Materials,"

[2]Peterson, L. D., and Hinkle, J. D., "What Limits the Achievable Areal Densities of Large Aperture Space Telescopes?," SPIE Paper Number 5899-11, 2005.

[3]Hedgepeth, J. M., "Support Structures for Large Infrared Telescopes," NASA Contractor Report 3800, 1984.

[4]Lake, M. S., Peterson, L. D., and Levine, M. B., "Rationale for Defining Structural Requirements for Large Space Telescopes," *Journal of Spacecraft and Rockets*, Vol. 39, No. 5, September-October 2002, pp. 674-681

[5]Mikulas, Jr., M. M., Bush, H. G., and Card, M. F., "Structural Stiffness, Strength and Dynamic Characteristics of Large Tetrahedral Space Truss Structures," NASA Technical Memorandum X-74001, March 1977.

[6]Hedgepeth, J. M., "Influence of Fabrication Tolerances on the Surface Accuracy of Large Antenna Structures," *AIAA Journal*, Vol. 20, No. 5, May 1982.

[7]Lake, Mark S., Peterson, Lee D., Mikulas, Martin M., "Space Structures on the Back of an Envelope: John Hedgepeth's Approach to Design," AIAA 2003-1448, presented at the 44th Structures, Structural Dynamics and Materials Conference, Norfolk, VA, 7-10 April 2003.

[8]Leissa, Arthur W., *Vibration of Plates*, NASA SP-160, 1969.

[9]Goodman, W., Jacoby, M., "Lightweight Athermal SLMS Innovative Telescope (LASIT) … and Latest Cryo-Data Results," presented at SPIE Conference 5528A-10, August 5, 2004.

[10]Kitipornchai, S., Liew, K. M., Xiang, Y, Wang, C. M., "Free Vibration of Isosceles Triangular Mindlin Plates," *International Journal of Mechanical Science*, Vol. 35, No. 2, pp.89-102, 1993.

[11]Nye, T.W., et al, "Performance of active vibration control technology: the ACTEX flight experiments," *Smart Mater. Struct*. 8 767-780, 1999.

[12]Fanson, J. F., Ealey, M., "Articulating Fold Mirror for the Wide-Field/Planetary Camera II," SPIE Vol. 1920 Active and Adaptive Optical Systems II, Albuquerque, NM, 1993.

[13]http://www.morganelectroceramics.com/

[14]http://www.xinetics.com/

[15]http://www.noliac.com/

[16]Lynch, C.S., "The Effect of Uniaxial Stress on the Electro-Mechanical Response of 8/65/35 PLZT," *Acta Mater*., 44(10), 4137-48 (1996).